Crystalline and quasi-crystalline phases of the Al-Si-Mn system: a comparison of the ^{57}Fe electric-field-gradient properties

1990 J. Phys.: Condens. Matter 2 6413

(http://iopscience.iop.org/0953-8984/2/30/007)

J. Phys.: Condens. Matter **2** (1990) 6413–6431. Printed in the UK

Crystalline and quasi-crystalline phases of the Al–Si–Mn system: a comparison of the ^{57}Fe electric-field-gradient properties

R A Brand†§ G Le Caër‡ and J M Dubois‡

† IFF der KFA Jülich, D-5170 Jülich, Federal Republic of Germany

‡ Laboratoire de Science et Génie des Materiaux Metalliques, (CNRS UA 159), Ecole des Mines, F-54042 Nancy Cedex, France

Received 4 December 1989, in final form 23 March 1990

Abstract. We present here the determination of the distribution $P(q)$ of the electric field gradient in Fe-doped Al–Si–Mn icosahedral and decagognal quasi-crystals and in the related crystalline phases, using in-field Mössbauer effect spectroscopy. The distribution $P(q)$ for the quasi-crystalline compounds shows a bimodal, nearly symmetric form with $P(0) \simeq 0$ and equal averages over positive and negative $q = \frac{1}{2}eQV_{zz}$, $-\langle q_- \rangle \simeq \langle q_+ \rangle$ and equal standard deviations: $\sigma_- \simeq \sigma_+$. The results for the majority sign of the distribution $P(q)$ will be compared to the results for the cubic, hexagonal and orthorhombic compounds. The results show that there are similarities in the local order between the icosahedral quasi-crystalline phase and the hexagonal phase. No evidence is found for a two-site model, which has recently been proposed by other authors.

1. Introduction

The discovery that sharp diffraction peaks with icosahedral (i-) symmetry could be observed in aluminium–manganese alloys with approximate composition $Al_{86}Mn_{14}$ [1] has provoked much work devoted to the determination of the structure of these new phases. Local techniques such as extended x-ray absorption fine structure (EXAFS) [2–5], nuclear magnetic resonance (NMR) [6, 7] and Mössbauer effect (ME) spectroscopy [8–11] have attracted some attention. From NMR the main findings are that these quasi-crystalline (QC) alloys show a distribution of electric field gradients (EFG) and asymmetry parameters η at the Al site. In addition, it was found that most but not all the Mn atoms carry a magnetic moment (with about 15% remaining magnetic) [7, 12]. At low temperatures, these Mn moments order at a spin-glass transition [13, 14].

The early binary alloys $Al_{86}Mn_{14}$ also contained noticeable amounts of FCC AlMn solid solution. Systematic investigations have shown that a single QC phase forms in ternary Al–Si–Mn [15]. Formation of the icosahedral quasi-crystal (i-QC) in Al–Si–Mn occurs however only within a very narrow concentration range [15, 16]: 20–23 at.% Mn and 4–6 at.% Si. For smaller Si contents, the Al_4Mn decagonal (T-) QC phase [17] grows at the expense of the icosahedral QC. In addition, crystalline phases are observed at

§ Present and permanent address: Laboratorium für Angewandte Physik, Universität Duisburg, Lotharstrasse 1, D-4100 Duisburg 1, Federal Republic of Germany.

0953-8984/90/306413+19$03.50

the limits of the i-QC domain, namely hexagonal β-$Al_{10-x}Si_xMn_3$ [18] in the vicinity of 4–8 at.% Si and 23 at.% Mn, and the cubic α-$Al_{19-x}Si_xMn_4$ [19,20] at higher Si concentrations. Recently Tibballs *et al* [21] have reviewed the question of the solubility of silicon in the cubic and hexagonal phases. The orthorhombic phase o-Al_6Mn [22] is stable without silicon substitution.

Addition of silicon significantly reduces the disorder of the icosahedral network and has a drastic effect on both the stability and the physical properties of the i-QC. Both x-ray [23] and electron [24] diffraction studies support this conclusion. The linewidth of the pseudo-Bragg peaks is smaller in the ternary Al–Si–Mn i-QC than in the binary Al–Mn i-QC [25], and this implies a longer coherence length associated with icosahedral order in the ternary. However, both neutron diffraction [26] and electron microscopy [27] demonstrate that disorder has not completely vanished in i-$Al_{74}Si_5Mn_{21}$, but shows instead that the silicon induces systematic spot displacements in the fivefold diffraction patterns [26]. Magnetism is the physical property most affected by the presence of silicon which changes the type of spin-glass behaviour at low temperatures compared with that of binary Al–Mn i-QC [28]. Ferromagnetic transitions have been reported for the Al–Si–Mn amorphous alloys [13] and in crystallised alloys [29], both for silicon contents of about 30 at.%.

These results suggest that a direct comparison of the local atomic order present in these different quasi-crystalline and crystalline phases is highly desirable. In this paper we report on studies of in-field Mössbauer spectroscopy of Fe-doped icosahedral and decagonal QC as well as the cubic (α-), hexagonal (β-) and orthorhombic (o-) Al–Si–Mn alloys. The early Mössbauer work consisted of studies of Fe-doped Al–Si–Mn i-QC as measured at room temperature and in zero magnetic field. Such spectra show broadened quadrupole split doublets. Swartzendruber *et al* [8] have evaluated such spectra assuming *a priori* that there are two sites present with relative concentrations given by the golden mean $\tau = (1 + \sqrt{5})/2$. The similar QC system i-$Al_{86}Cr_{14-x}Fe_x$ (with $3 \leq x \leq 14$) has recently been reported on by Dunlap *et al* [30] who also used a two-site fit. They showed that the relative areas of the two doublets depend on the iron concentration and concluded from this fact that this shows evidence for preferred site occupancy of Fe. However, both we [31] and others [11,32] have shown that the zero-field spectra of quasi-crystalline phases are not sufficiently resolved to detect any possible preferred occupancy. This lack of sensitivity is due to the presence of significant disorder. The decagonal phase has been studied by Mössbauer spectroscopy both in zero [33,34] and in external field [35]. More information can be obtained from in-field ^{57}Fe ME spectra, which we present below since in this case, the positive and negative EFG terms can be distinguished. It is necessary to treat the ME spectra of the icosahedral and decagonal QC phases as composed of a distribution of EFG effects, and the results of such a treatment do not confirm the two-site models. In somewhat more detailed work, Eibschütz *et al* [9] analyzed the zero-field spectra in terms of the Czjzek shell model distribution [36]. They concluded that the local environments of Mn (and Fe) in the amorphous and quasi-crystalline alloys are similar. A further problem is that in the case of Al-based alloys, the presence of short ranged chemical order is not necessarily detected in the presence of sufficient medium and long range disorder [37]. In addition, Scholte *et al* [38] have also shown that in the case of amorphous alloys, changes detected in the EFG distribution can be of electronic and not of structural origin.

Thus the interpretation of EFG distributions is sometimes not very straightforward. We need a reference system for the EFG distribution in the case of complete disorder,

and an indication of the changes in this model distribution with growing characteristic local order. In a pioneering work, Czjzek *et al* [36] made numerical simulations of the EFG joint distribution $P(q,\eta)$ for randomly filled atomic shells in a point charge calculation. It was shown by Le Caër *et al* [31, 39] that in fact this distribution results from very general statistical considerations. It is only necessary to consider that (i) the solid is macroscopically isotropic in the statistical sense and (ii) the elements of the EFG tensor V_{ij} are distributed according to a multivariate Gaussian law. Le Caër *et al* [31] have called this the Gaussian isotropic model (GIM); this model is reviewed in the appendix. The resulting joint distribution function $P(q,\eta)$ is written as:

$$P(q,\eta) = \frac{q^4\eta}{\sigma^5\sqrt{2\pi}}\left(1-\frac{\eta^2}{9}\right)\exp\left[-\frac{q^2}{2\sigma^2}\left(1+\frac{\eta^2}{3}\right)\right] \tag{1}$$

with $q = \frac{1}{2}eQV_{zz}$. Here V_{zz} and the asymmetry parameter η are defined in the used way, with

$$|V_{zz}| \geq |V_{yy}| \geq |V_{xx}| \tag{2a}$$

$$\eta = |(V_{yy} - V_{xx})/V_{zz}| \in \{0,1\} \tag{2b}$$

and where $V_{xx} + V_{yy} + V_{zz} = 0$ holds for the principal components of the EFG tensor. Please note that in Le Caër *et al* [31] there was an error in the definition of the constant $a = 5/(2\langle S^2\rangle) = 1/(2\sigma^2)$. In equation 10 of that work, $a = 1/(3\sigma^2)$ was used but not indicated. From $P(q,\eta)$ we can calculate the two marginal distributions

$$Q(q) = \int_0^1 P(q,\eta)\,\mathrm{d}\eta$$

$$R(\eta) = \int_{-\infty}^{+\infty} P(q,\eta)\,\mathrm{d}q.$$

These two are given in figure 1. We see that there is zero probabilty of finding $q = 0$ (cubic or higher symmetry) or $\eta = 0$ (cylindrical symmetry). $Q(q)$ is bimodal with symmetric parts for $q < 0$ and $q > 0$. Since ^{57}Fe ME spectra are relatively insensitive to small changes in η, it is sufficient to take an average value $\langle\eta\rangle \simeq 0.6$, as has been shown by Le Caër *et al* [40]. The modulus $\Delta E_Q \equiv \Delta$ of the zero-trace EFG tensor can be written as

$$\Delta^2 = (\tfrac{1}{2}eQ)^2 \sum_{i=x,y,z} V_{ii}^2 = q^2\left(1+\frac{\eta^2}{3}\right) \tag{3}$$

where the factor $\frac{1}{2}eQ$ is for units (where Q is the nuclear quadrupole moment and q is defined above). The distribution of Δ can be written as

$$P(\Delta) = \frac{1}{3}\sqrt{\frac{2}{\pi}}\frac{\Delta^4}{\sigma^5}\exp\left(-\frac{\Delta^2}{2\sigma^2}\right). \tag{4}$$

The marginal distribution $Q(q)$ can be written as

$$Q(q) = \frac{1}{\sigma}\sqrt{\frac{2}{\pi}}\left[\left(\frac{3q^2}{2\sigma^2}-1\right)\exp\left(-\frac{q^2}{2\sigma^2}\right) + \left(1-\frac{4q^2}{3\sigma^2}\right)\exp\left(-\frac{2q^2}{3\sigma^2}\right)\right]. \tag{5}$$

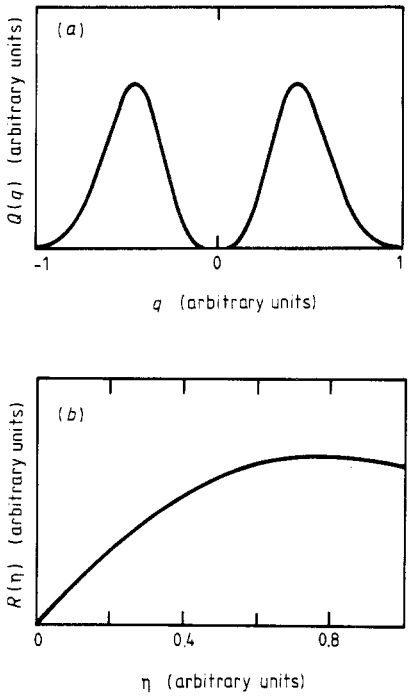

Figure 1. Marginal distributions (*a*) $Q(q)$ and (*b*) $R(\eta)$ from the Czjzek shell model with $\beta = 0$.

The effect of short-range correlations has been studied both by Czjzek *et al* [36] and by Le Caër *et al* [40]. Any changes in the distribution function due to such correlations should be most pronounced for the first atomic shell. Czjzek *et al* made numerical simulations of the effect of the excluded volume due to finite atomic size within one atomic shell. They find that the simulations can be best represented by an additional cubic term in $P(q, \eta)$ of $1 + \beta q^3(1 - \eta^2)/\sigma^3$. The factor β represents the excluded volume effect, and this results in a distribution that is asymmetrical with respect to positive and negative EFG. The area of the positive part of the distribution

$$p_+ = \int_0^{+\infty} Q(q)\,\mathrm{d}q$$

is given by

$$p_+ \simeq \frac{1}{2} + \sqrt{\frac{32}{\pi}}\beta \tag{6}$$

for $|\beta| \leq 0.05$. This means that the sign of β is the sign of the dominating EFG in the distribution over q.

In a different approach, Le Caër *et al* [31] have studied the problem of how the spectral properties of a fixed Hamiltonian $\mathcal{V}_0$ are perturbed by the addition of a random interaction $\lambda\mathcal{V}_G$. This $\mathcal{V}_G$ (belonging to the Gaussian orthogonal ensemble) can dominate over $\mathcal{V}_0$ when the norm of $\lambda\mathcal{V}_G$ is larger than the norm of $\mathcal{V}_0$. This approach was inspired by a similar method used in nuclear physics [41]. There are

also certain similarities to the spin-glass problem when we consider the transition from spin glass (domination by λV_G) to ferromagnetic order (domination by V_0) [42]. Le Caër *et al* find a progressive change in the distribution towards a more narrow form so that the ratio $\langle\Delta\rangle/\sigma_\Delta$ increases from the lower limiting value of 3.094 given by the GIM, where $\langle\Delta\rangle$ is the average of Δ over $P(\Delta)$ and σ_Δ is the standard deviation of Δ.

Recently Levi Yeyati *et al* [43] have calculated EFG distributions numerically for the Zr sites in amorphous $Zr_{70}Cu_{30}$ alloys and compared these with the calculated EFG in crystalline Zr_2Cu. They find very similar marginal distributions $Q(q)$ and $R(\eta)$ as in the shell model with non-zero β, and find $\langle\eta\rangle \simeq 0.6$ as well. The sign of β agrees with the sign of V_{zz} found for the crystalline compound in a similar calculation.

In the case of ^{57}Fe ME spectroscopy, it is necessary to study spectra taken in an external magnetic field in order to separate positive and negative EFG terms. Recently we have published first results [31] showing that the dominant EFG sign in the Fe-doped Al–Si–Mn icosahedral quasi-crystal and the sign of the EFG in the hexagonal crystalline compound are both negative and have similar magnitudes. In this work the cubic phase was studied as well, but the sign of the EFG at the two Mn (Fe) sites was not determined. In addition, the results for the zero-field spectrum of this sample were ambiguous and two different solutions were possible. The cubic and hexagonal phases are composed either of stacking sequences of Mackay icosahedra [44–46], or of fragments of such polyhedra. These structures have often been used as the first approximation to the quasiperiodic structures of Al–Si–Mn i-QC. Eibschütz *et al* [10] have also studied in-field ME spectra of Fe-substituted Al–Si–Mn i-QC without obtaining the sign of the dominating EFG or the distribution $P(q)$. They have concluded that Fe substitutes only in non-magnetic Mn sites from the fact that the internal and external magnetic fields are the same. We have studied the magnetic properties of the Fe-substituted hexagonal phase and have shown that, even in this case, where the magnetic order is due to the presence of Fe, the internal and external magnetic fields are equal for in-field spectra [47] due to the fact that the magnetic moments are small, and in an antiferromagnetic or spin-glass state. It is thus questionable to reach such conclusions for the Fe substitution on the basis of even in-field spectra. We want to stress that these QC spectra have been evaluated using the exact (static) Hamiltonian averaged over an isotropic EFG texture and including the effect of the distribution over V_{zz}.

2. Experimental details

Melt-spun alloys have been prepared of icosahedral quasi-crystalline phases, which we shall denote as i-$Al_{5.6}Si_\epsilon$(MnFe), i-$Al_{4.8}Si_\epsilon$(CrFe) and i-Al_4(MnFe), and the decagonal QC phase T-Al_4(MnFe). In addition, melt-spun samples of the cubic α-$Al_{16}Si_3(MnFe)_4$, hexagonal β-$Al_9Si(MnFe)_3$ and orthorhombic o-Al_6(MnFe) crystalline phases have been prepared as well. In this notation, (MnFe) stands for $(Mn_{0.72}Fe_{0.28})$, and (CrFe) stands for $(Cr_{0.5}Fe_{0.5})$. The silicon addition $\epsilon \simeq 0.06$ stabilises the i-QC phases. Table 1 shows the nominal compositions including the silicon content. All samples have been characterised by x-ray diffraction [48,49], and the QC [48,49] and hexagonal phases [47] have been studied by neutron diffraction. Here we present results on the distributions $P(\Delta)$ from the zero-field and $P(q)$ from in-field ME spectra calculated using a histogram method.

The ME spectra were taken using a ^{57}Co–Rh source at room temperature (for the cubic phase, the source for the in-field spectrum was at 4.2 K). The in-field spectra have

Table 1. Nominal compositions of the samples and notation used in the text.

Notation	Nominal composition
i-$Al_{5.6}Si_{\epsilon}$(MnFe)	$Al_{84}Si(Mn_{0.72}Fe_{0.28})_{15}$
i-$Al_{4.8}Si_{\epsilon}$(CrFe)	$Al_{82}Si(Cr_{0.5}Fe_{0.5})_{17}$
i-Al_4(MnFe)	$Al_{80}(Mn_{0.72}Fe_{0.28})_{20}$
T-Al_4(MnFe)	$Al_{80}(Mn_{0.72}Fe_{0.28})_{20}$
α-$Al_{16}Si_3$(MnFe)$_4$	$Al_{71.5}Si_{12.4}(Mn_{0.72}Fe_{0.28})_{16.1}$
β-Al_9Si(MnFe)$_3$	$Al_{74}Si_6(Mn_{0.72}Fe_{0.28})_{20}$
o-Al_6(MnFe)	$Al_{85.7}(Mn_{0.72}Fe_{0.28})_{14.3}$

been treated using the exact Hamiltonian for mixed hyperfine magnetic and electric quadrupole interactions. The algorithm used to calculate subspectra depended upon the assumed relationship between the direction of the hyperfine magnetic field B_{hf} and the direction of the EFG principal axes. For the case of a fixed angle between B_{hf} and the EFG axes, the algorithm of Ruebenbauer and Birchall [50] was used. In the case of no correlation between the direction of B_{hf} and the EFG axes (isotropic EFG texture), the algorithm of Blaes *et al* [51] was used. The EFG distribution $P(q)$ has been calculated from the spectra for the QC using a modified Hesse–Rübartsch formalism [52–54] which accepts only positive $P(q)$ and iterates in a non-linear manner for all parameters except the distribution $P(q)$. This includes the isomer shift I_S and the standard deviation of the distribution in I_S, denoted as σ_I. For the QC, only the algorithm of Blaes *et al* is appropriate. In order to conserve computation time, the theoretical subspectra are calculated at fixed intervals of q, and for a fixed hyperfine magnetic field B_{hf} and asymmetry parameter $\eta = 0.6$. These are stored in a numerical file., and the fit program uses this file to calculate $P(q)$. Spline coefficients are used to interpolate such fixed theoretical spectra for the actual isomer shift. In order to check the objectivity of these distributions, we have also used a new maximum entropy method as well [55], and the results are very similar. In the following, the isomer shift is reported as referenced to that of BCC Fe at room temperature. The zero velocity of the spectra shown is that of the source.

3. Results

We first discuss the results for the icosahedral and decagonal QC phases. The spectra at 4.2 K in zero and in external field (5 T, perpendicular to the γ-ray direction) are shown in figure 2 for i-$Al_{5.6}Si_{\epsilon}$(MnFe), figure 3 for i-$Al_{4.8}Si_{\epsilon}$(CrFe), figure 4 for i-Al_4(MnFe) and figure 5 for T-Al_4(MnFe). The theoretical fits have been obtained by the histogram distribution of $\Delta E_Q \equiv \Delta$ (zero-field spectra) and q (with $\eta = 0.6$; in-field spectra). We have assumed as well a (small) isomer shift distribution independent of the EFG by including the standard deviation parameter σ_I. The slight asymmetry seen in the zero-field spectrum of T-Al_4(MnFe), figure 5 (upper), was compensated for by using a small linear correlation between isomer shift and quadrupole splitting. The in-field spectrum was much easier to fit, as seen from figure 5 (lower). The distributions $P(\Delta)$ and $P(q)$ are shown to the right of the respective spectra. The distributions $P(q)$ are all bimodal in character but with dominant negative (i-QC) or positive (i-QC) sign. It should be noted that the dominant negative sign for the i-QC samples is well outside experimental errors, but that this is not the case for the positive sign found for the

T-QC sample. The distributions for the two i-QC samples show evidence for a small contribution near $q = 0$. This will be discussed in conjunction with the presence of small amounts of FCC Al in these samples, containing some dissolved Fe.

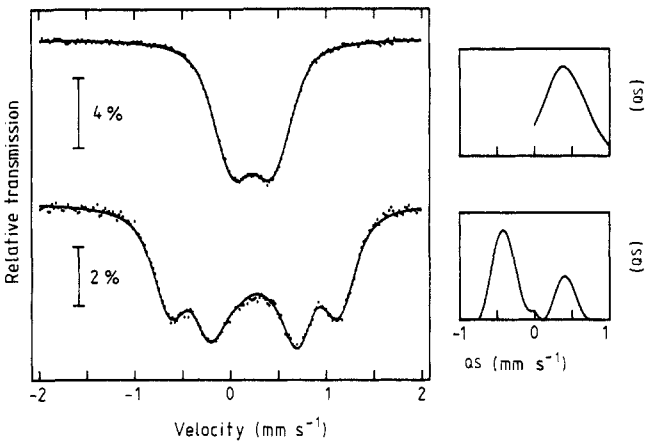

Figure 2. (*a*) ME spectra and (*b*) resulting distributions for the i-QC sample i-$Al_{5.6}Si_6$(MnFe) at $T = 4.2$ K: (upper) zero-field and (lower) in-field; $B_{ext} = 5$ T, perpendicular to γ-ray. The distributions $P(\Delta)$ from the upper, and $P(q)$ from the lower spectrum are shown to the right.

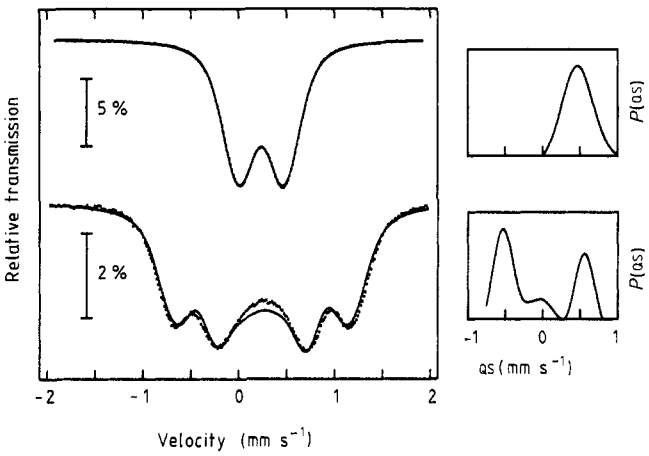

Figure 3. (*a*) ME spectra and (*b*) resulting distributions for the i-QC sample i-$Al_{4.8}Si_6$(CrFe) at $T = 4.2$ K: (upper) zero-field and (lower) in-field, $B_{ext} = 5$ T perpendicular to γ-ray. The distributions $P(\Delta)$ from the upper and $P(q)$ from the lower spectrum are shown to the right.

Results for the average isomer shift $\langle I_S \rangle$, standard derivation σ_I, as well as averages over the zero-field distribution $P(\Delta)$ are shown in table 2. Table 3 presents results for the in-field spectra. There p_+ is the average over the positive, and p_- over the negative part of $P(q)$. In the same way, the averages $\langle q_+ \rangle$ and $\langle q_- \rangle$ and standard deviations σ_+ and σ_- can be defined from the integral first and second moments over $P(q)$ for $q \geq 0$ or $q \leq 0$ respectively.

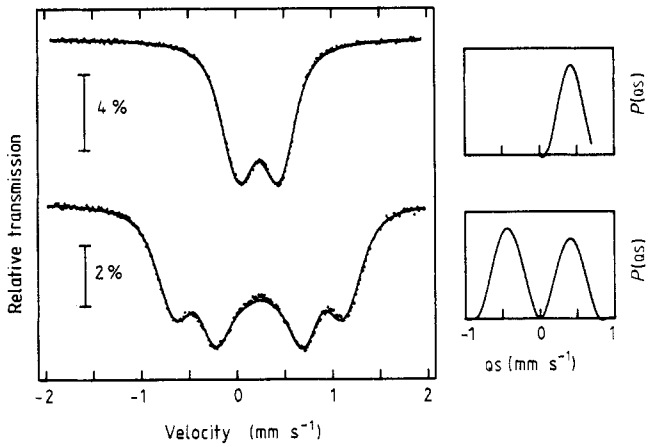

Figure 4. (*a*) ME spectra and (*b*) resulting distributions for the i-QC sample i-Al_4(MnFe) at T = 4.2 K: (upper) zero-field and (lower) in-field, B_{ext} = 5 T perpendicular to γ-ray. The distributions $P(\Delta)$ from the upper and $P(q)$ from the lower spectrum are shown to the right.

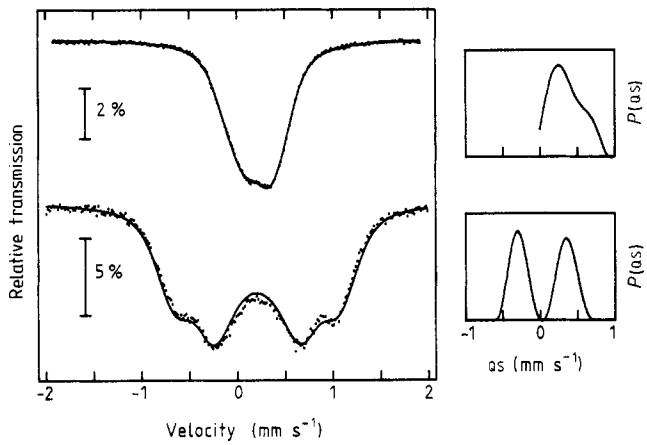

Figure 5. (*a*) ME spectra and (*b*) resulting distributions for the T-QC sample T-Al_4(MnFe) at T = 4.2 K: (upper) zero-field and (lower) in-field, B_{ext} = 5 T perpendicular to γ-ray. The distributions $P(\Delta)$ from the upper and $P(q)$ from the lower spectrum are shown to the right.

Table 2. Results for the QC phases from the zero-field spectra at 4.2 K. Units for I_S, σ_I, $\langle\Delta\rangle$, and σ_Δ are mm s^{-1} and errors about $\pm$0.005 mm s^{-1}.

Sample	I_S	σ_I	$\langle\Delta\rangle$	σ_Δ	$\langle\Delta\rangle/\sigma_\Delta$
i-$Al_{5.6}Si_6$(MnFe)	0.353	~0.00	0.430	0.244	1.76
i-$Al_{4.8}Si_6$(CrFe)	0.346	0.052	0.477	0.183	2.61
i-Al_4(MnFe)	0.351	0.078	0.422	0.132	3.19
T-Al_4(MnFe)	0.337	~0.00	0.357	0.215	0.175

Table 3. Results for the QC phases from the in-field spectra at 4.2 K. Units for I_S, σ_I, $\langle q_\pm \rangle$ and $\sigma_{q_\pm}$ are mm s^{-1} and errors about ± 0.005 mm s^{-1}; units for $p_\pm$ are %.

Sample	I_S	σ_I	$\langle q_+ \rangle$ $\langle q_- \rangle$	σ_{q+} σ_{q-}	$\langle q_+ \rangle / \sigma_{q+}$ $\langle q_- \rangle / \sigma_{q-}$	p_+ p_-
i-$Al_{5.6}Si_\epsilon$(MnFe)	0.353	0.066	0.397	0.136	2.92	29.7
			−0.402	0.140	2.87	70.3
i-$Al_{4.8}Si_\epsilon$(CrFe)	0.347	0.040	0.487	0.196	2.48	39.1
			−0.493	0.167	2.95	60.9
i-Al_4(MnFe)	0.351	0.055	0.412	0.150	2.74	45.2
			−0.422	0.157	2.69	54.8
T-Al_4(MnFe)	0.323	0.130	0.358	0.188	3.03	50.2
			−0.298	0.108	2.75	49.8

The zero- and in-field ME spectra for the crystalline phases are given in figure 6 for the cubic phase, figure 7 for the hexagonal phase and figure 8 for the orthorhombic phase. The hexagonal phase has been studied at $T = 110$ K (zero-field) and at 122 K (in-field) in order to avoid any effect of the magnetic transition at lower temperature [47]. Results are given in table 4 for these three compounds, as obtained using the Blaes *et al* algorithm for the in-field spectra.

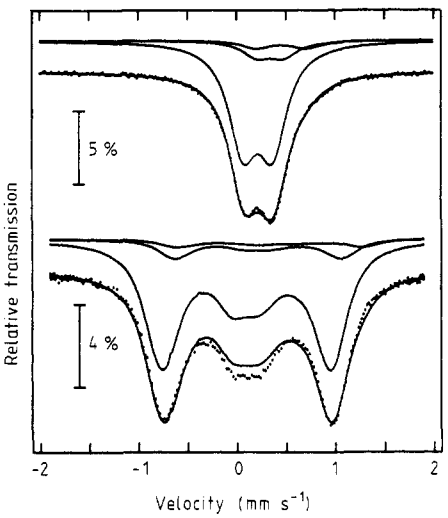

Figure 6. ME spectra for the cubic phase α-$Al_{16}Si_3(MnFe)_4$ at $T = 4.2$ K in (upper) zero field and (lower) a field of $B_{ext} = 5$ T parallel to the γ-ray.

The zero-field ME spectrum for the cubic phase α-$Al_{16}Si_3(MnFe)_4$ gave ambiguous results [31] for the Fe-substitution in the two Mn sites with two different possible relative areas, either in ratio of 3:1 or 2:1. Since the two Mn sites are in the ratio of 1:1, there is certainly preferred site substitution of Fe. The in-field results for this compound have been used to resolve this ambiguity. The results are given in table 4.

The hexagonal β-$Al_9Si(MnFe)_3$ spectra shown in figure 7 (upper) were taken above the known magnetic phase transition at 80 K [47]. The upper zero-field spectrum has been taken in standard transmission geometry to show the effect of texture common to hexagonal systems. For the other spectra, this sample has been studied in magic

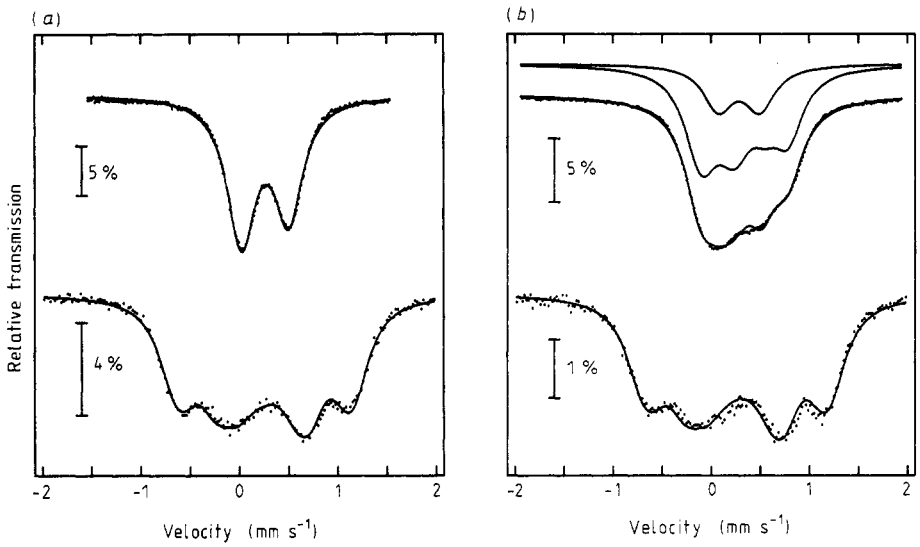

Figure 7. ME spectra for the hexagonal phase β-$Al_9Si(MnFe)_3$: (*a*) in the paramagnetic state at (upper) $T = 110$ K, zero field, and (lower) $T = 122$ K, in an external field of $B_{ext} = 5$ T perpendicular to the γ-ray and (*b*) in the magnetic state at $T = 4.2$ K, in (upper) zero field, and (lower) external field $B_{ext} = 5$ T perpendicular to the γ-ray.

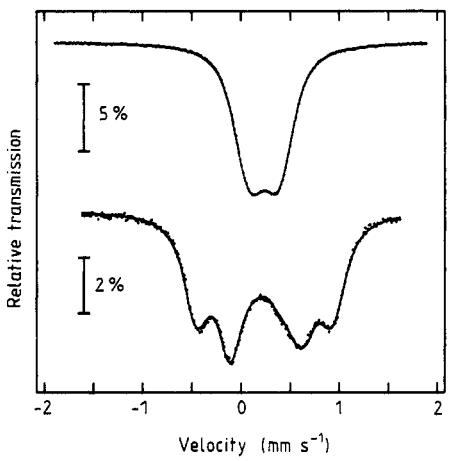

Figure 8. ME spectra for the orthorhombic phase o-$Al_6(MnFe)$ at $T = 4.2$ K in (upper) zero field and (lower) an external field of $B_{ext} = 4$ T perpendicular to the γ-ray.

angle geometry [56] both in zero and in magnetic field in order to avoid these problems. The in-field spectrum (external field $B_{ext} = 5$ T, perpendicular to γ-ray) yielded an internal hyperfine field of $B_{int} = 4.71$ T, and a quadrupole effect of $q = -0.44$ mm s^{-1} with $\eta = 0.88$ as evaluated with the Blaes *et al* algorithm (B_{int} fixed in space; V_{zz} oriented randomly). In figure 7 (lower) we have shown spectra at 4.2 K in zero field (upper) and for $B_{ext} = 5$ T (perpendicular to γ-ray direction; lower). These have been evaluated using two different algorithms. For the in-field spectrum the Blaes *et*

al routine was used as in the above. We find $B_{int} = 4.97$ T, very close to the value of the external field, and $q = -0.462$ mm s^{-1} with $\eta = 0.79$, in good agreement with the results above at $T = 122$ K. For the zero-field spectrum, this procedure did not yield adequate results. It was found that assuming a fixed orientation of the hyperfine field B_{hf} within the EFG axis yielded better results. In addition, a 25% non-magnetic contribution with identical $\Delta = |q|\sqrt{1+\eta^2/3}$ but with $B_{hf} = 0$ was found. For the magnetic part, the angle between B_{hf} and V_{zz} was found to be 90° (isotropic B_{hf} and V_{zz} but with a fixed relative angle), $q = -0.38$ mm s^{-1}, and $\eta = 0.3$. This value of η is probably less reliable than that from the in-field spectrum at $T = 122$ K, Fig 7 (upper). The zero- field spectrum yielded $B_{hf} = 2.3$ T for the magnetic part.

Table 4. Results for the crystalline phases from the in-field spectra. Units for I_S and q are mm s^{-1} and errors about ±0.05 mm s^{-1}; units for area are %. Isomer shift I_S is at 4.2 K, referenced to BCC Fe at room temperature.

Sample	Area	I_S	q	η
α-$Al_{16}Si_3(MnFe)_4$				
site 1	82	0.32	−0.30	0.6
site 2	12	0.44	0.27	0.6
site 3	6	0.55	0.5	—
β-$Al_9Si(MnFe)_3$	—	0.358	−0.460	0.8
o-$Al_6(MnFe)$	—	0.351	+0.281	0.4

In table 4 we give the results for the orthorhombic phase as well; a value $\eta = 0.44 \pm 0.02$ has been found by fitting with the Blaes *et al* routine. This is similar to the value of 0.4, which we have published earlier [31].

4. Discussion

The i-QC samples unavoidably contain some FCC Al, and it is also known that Al can contain considerable amounts of Mn [57] and Fe [58] in metastable solid solution. The composition of the icosahedral phase was accurately determined by referring to neutron diffraction results [59]. This results in a composition of $Al_{4.30}Si_{0.06}(Mn_{0.72}Fe_{0.28})_1$ for the sample i-$Al_{5.6}Si_\epsilon$(MnFe), and a composition of $Al_{4.44}Si_{0.06}(Cr_{0.5}Fe_{0.5})_1$ for the sample i-$Al_{4.8}Si_\epsilon$(CrFe). This FCC Al seems to be the cause of the small excess intensity at low (but negative) values of q observable in the distributions $P(q)$ for the i-QC samples, figures 2 (lower) and 3 (lower). The compositions of the quasi-crystalline phases of the other two samples i-Al_4(MnFe) and T-Al_4(MnFe) are not known, but should be very close to the nominal compositions, since no other residual phases were detected in these samples. (It is known that the icosahedral structure has a small but definite stoichiometry range between $Al_{4.5}Si_{0.06}Mn_1$ and $Al_{4.1}Si_{0.06}Mn_1$ [26].) The distributions $P(q)$ in figures 4 (lower) and 5 (lower) do not show any low q excess intensity, as was the case for the two i-QC samples. The nominal composition of the cubic α phase (table 1) is close to $Al_{21}Mn_4$ while the ideal end-member is $Al_{19}Mn_4$ [19] and there is indeed some FCC Al phase present as well in this sample, with Mn and Fe in solid solution. We have found three quadrupole doublets at $T = 4.2$ K in the zero-field spectrum [31], where the small additional spectrum (see figure 6 (upper) and table 4) given as site 3 probably represents the additional phase. In order to evaluate

the in-field spectrum (figure 6 (lower)), we have fixed the value of the quadrupole splitting q, the isomer shift I_S and the relative depths to the values given by the zero-field spectrum, and then checked for the sign of the different values of q, and the value of the asymmetry parameter η. The choice $q < 0$ for site 1, and $q > 0$ for site 2 have thus been determined. The choice for site 3 was not significant.

The zero-field ME spectra of the three QC phases yield distributions $P(\Delta)$ that could be represented by two different values Δ_1 and Δ_2, as has been proposed by Swartzendruber *et al* [8]. Dunlap *et al* [30] have used such two-site evaluations for zero-field spectra and have used these results to conclude that there is preferential site substitution of Fe in icosahedral Al–Mn alloys. Similar results for the decagonal QC phases have been reported on by Koopmans [34] and by Gupta [33]. If this type of model were correct, we would expect a bimodal $P(q)$ with two different maxima, but without the almost symmetrical form that we have obtained (figures 2, 3, 4 and 5). There would also not be any reason for the sign of V_{zz} to be different at the two different sites. In fact, if we fit the zero-field spectra with two quadrupole doublets, the resulting values of Δ_1 and Δ_2 are not at all consistent with the values $\langle q_+ \rangle$ and $\langle q_- \rangle$ as determined from the in-field spectra. It seems clear from our measured $P(q)$ that in fact the Czjzek shell model or GIM form is a much better starting point to understand these spectra. In this picture, we look for an asymmetry in area between the positive and negative parts of $P(q)$ to determine the dominating EFG sign.

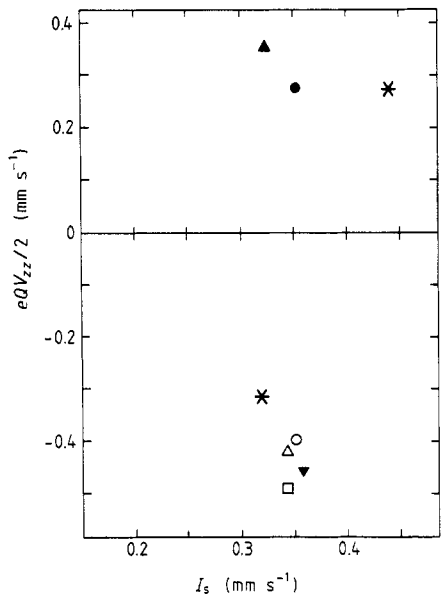

Figure 9. The comparison of the EFG effect $q = \frac{1}{2}eQV_{zz}$ and the isomer shift I_S at $T = 4.2$ K for the crystalline phases with the majority part of the $P(q)$ distribution for the QC phases: (○) i-$Al_{5.6}Si_\epsilon$(MnFe); (□) i-$Al_{4.8}Si_\epsilon$(CrFe); (△) i-Al_4(MnFe); (▲) T-Al_4(MnFe); (*) α-$Al_{16}Si_3(MnFe)_4$, two sites; (▼) β-Al_9Si(MnFe)$_3$; (●) o-Al_6(MnFe).

We then compare this majority EFG sign and magnitude, and the isomer shift to the known results for the crystalline phases. First we notice from table 2 that the majority sign for the icosahedral QC phases is negative while that for the decagonal

phase is positive (where it should be noted that the T-QC result is actually very close to 50:50). In figure 9 we plot the results for q and I_S for all the phases reported on here. In the case of the QC phases, the majority part of P(q) is shown, while for the cubic phase, both sites are shown. A certain similarity is found between the results (I_S, q) for the icosahedral QC phases and that of the hexagonal phase. The results for the i-QC samples are grouped around the result for the hexagonal phase. The site of the cubic phase with a negative EFG shows a smaller isomer shift and a smaller EFG effect (in absolute value). The other site shows a positive EFG effect and a much larger isomer shift. The orthorhombic phase shows a similar isomer shift, but a positive EFG effect. Using these hyperfine properties, we can say that the local environment found around the Mn (Fe) sites in the icosahedral QC is closest to that found in the hexagonal phase among the crystalline phases studied here.

Both the Czjzek shell model and the GIM give definite predictions on the ratio of average values to the standard deviation. These are given by $q_{\pm}/\sigma_{q_{\pm}} = \pm 3.047$ and $\langle\Delta\rangle/\sigma_{\Delta} = 3.094$. From the results of Le Caër *et al* [40] (see the appendix) these ratios should increase when $P(q)$ is dominated by a fixed EFG term. From the results given in table 2, we see that the experimental values are smaller than the theoretical lower limits, being in the range of about 2–3. For the in-field spectra, we obtain a ratio $|\langle q_{\pm}\rangle/\sigma_{q_{\pm}}|$ in the range of 2.5 to 3, in better agreement with the predictions of the GIM. These results have been obtained even despite the fact that we have optimised the value of the standard deviation σ_I of the isomer shift, and have used the experimental linewidth given by calibration spectra. It seems most likely however that σ_I should in fact be larger, which would decrease the standard deviations of the EFG effect σ_{Δ} and $\sigma_{q_{\pm}}$. In any event, the existence of local order is seen only in the asymmetry in area between positive and negative values of q.

For three different i-QC samples, we have obtained a preponderance of negative EFG values. This result must be judged with some caution, however, owing to the presence of Fe dissolved in the FCC Al also present. We estimate (using the measured lattice parameters of the FCC part) an upper limit of about 10% of the ME area in the i-$Al_{5.6}Si_{\epsilon}$(MnFe) and the i-$Al_{4.8}Si_{\epsilon}$(CrFe) samples is due to this phase. It is known [58] that the zero-field spectrum of Fe in FCC Al consists of a singlet and a doublet. Assuming that these contribute to the negative part of $P(q)$, the area asymmetry of the quasi-crystal would be somewhat smaller than that which is reported here for the sample i-$Al_{5.6}Si_{\epsilon}$(MnFe), but this would not qualitatively change our results since this would not be large enough to change the sign of the majority EFG term, even in the least favourable case. The FCC Al contribution for the i-Al_4(MnFe) and T-Al_4(MnFe) samples is not known, but is obviously negligible considering the x–ray diffraction results, which did not show any visible lines of this phase, and no excess contribution at low EFG q values was found. The result for the T-QC is however very close to equal areas for the positive and negative parts. This seems to show that there is in fact more disorder in T-QC structures than in i-QC. This is similar to the neutron difraction results for the ternary and binary i-QC structures discussed above: the binary i-QC show a shorter coherence length of the icosahedral order.

It is also a property of the dominating disorder on the spectrum of EFG values that the asymmetry parameter η is distributed as well. The characteristic property of this distribution in the shell model and in the GIM is that $R(\eta = 0) = 0$; that is there is zero probability of finding a site with cylindrical symmetry. From the known insensitivity of ^{57}Fe ME spectra to the value of η, it is sufficient in these types of QC spectra to set $\eta = \langle\eta\rangle \simeq 0.6$ as has been demonstrated before [40]. Xu *et al* [35] have found that the

in-field ME spectra of the decagonal alloy $Al_7(Mn_{0.7}Fe_{0.3})_2$ gave results with $\eta > 0$. This result is due to the dominating disorder in these quasiperiodic structures, and not to the type of local symmetry of the Fe site, as was concluded by the authors. The fivefold or tenfold global symmetry in these quasiperiodic structures does not imply that $\eta = 0$ since there is no such exact point symmetry for each site, except in the case of strictly nearest neighbour interactions only. Henley [60] has analyzed the spherical packings and local environments in Penrose lattices in both two and three dimensions (2D, 3D). This would be the most simple of all possible QC structure. Despite this, there are 24 distinct types of vertex configurations in 3D. Thus if we only consider the most local environment to calculate the spectrum of EFG values, there are 24 distinct configurations that contribute. Considering more distant neighbours would greatly increase this number, so that it is reasonable to expect that even with full site occupancy on a 3D Penrose lattice, the spectrum of EFG values would probably be similar to that for an amorphous structure of random close packing. This is the justification to use the GIM as a starting point to analyse our ME spectra for the EFG distribution.

Janot and Dubois [26, 61, 62] have used contrast variation on the Mn sites to determine the atomic decoration of Al–Si–Mn quasi-crystals by neutron diffraction. (The samples reported on here are actually from these studies.) This method makes no reference to any specific QC lattice model (except for the Bravais lattice, which is taken as a primitive hypercubic in 6D). They find that manganese atoms occupy the vertices of Penrose tiles in 3D. These form a well ordered subset with only one type of site, but with many different local configurations. The (Al, Si) atoms are located on the rhombic faces and on the triad axes of the prolate rhombohedron [63, 64]. Occupancy of these latter sites is fractional, thus embodying the necessary chemical modulation to allow for stability. It is found that there are only very few complete Mackay icosahedra present while most Mn atoms belong to triangular 'fragments' of this polyhedron, a figure that has certain similarities to the configuration found in hexagonal β-Al_9SiMn_3. There is however much disorder in the structure of this system despite the fact that angular correlations are retained. This disorder is due to the partial site occupation and to a certain variation in the exact positions of the (Al, Si) atoms [63, 65].

Considering this information on the atomic decoration, it is not surprising that the distribution of EFG terms deviates only slightly from the GIM distribution given by equation (1) and justified in the appendix on very general grounds.

5. Conclusions

We have presented results on the distribution of the ^{57}Fe EFG in a series of icosahedral and decagonal quasi-crystalline alloys. These have been compared with the EFG measured in cubic, hexagonal and orthorhombic Fe-doped Al–Si–Mn alloys. It has been shown that the two sites models used to demonstrate preferred Fe site substitution in such alloys are not confirmed by more detailed calculations of the distribution $P(q)$ obtained from in-field ME spectra. The form of $P(q)$ was found not to deviate very much from that given by the shell model or Gaussian independent model distribution. The major effect of local order is to change the relative areas of the positive and negative parts of the bimodal $P(q)$.

There was a correlation found between the sign of the dominating EFG part of the $P(q)$ for the QC phases and the sign of the EFG for the crystalline phases. This

was combined with the different isomer shifts to show the similarity between the icosahedral QC and the hexagonal phases. There is less similarity between either of the two sites in the cubic phase and the decagonal or icosahedral QC phases. These correlations are not related to the amount of silicon, since the decagonal phase forms with less than, and the cubic phase with more than, that for either the icosahedral QC or the hexagonal phase. There seems to be much more disorder in the decagonal structure, as evidenced by the fact that there was only very little asymmetry between positive and negative values of q in the distribution $P(q)$.

Acknowledgment

Thanks are due to Mr P Weinland (Ecole des Mines, Nancy) for the preparation of the samples.

Appendix. The shell and Gaussian isotropic models

Shell model

The functional form of the joint distribution $P(q,\eta)$ for random systems was first given by Czjzek *et al* [36] in an isotropic shell model. They show that the numerical simultations yield marginal distributions $Q(q)$ and $R(\eta)$ very close to those calculated from $P(q,\eta)$ given in equation (1), in the case where no account is made of finite atom size in filling the shell of atoms. When excluded volume effects are included, the simulations show different integral areas for positive and negative values of q. This can be understood from the following reasoning, where for the sake of argument we take positive charged ions. In this case a positive value of q results from a concentration of ions along one axis. A negative value of q results from a similar concentration, but along a ring. Owing to the finite size of the ions, this latter must be more probable, so that we should observe a preponderance of negative q values, which is what Czjzek *et al* obtain from simulation. They show that this can be represented to first order in the distribution $P(q,\eta)$ by including the cubic factor $1+\beta q^3(1-\eta^2)/\sigma^3$. Even in the presence of excluded volume effects, they report that $Q(q=0)=0$ and $R(\eta=0)=0$, indicating no presence of cubic or axial symmetry.

Gaussian isotropic model

We review the Gaussian isotropic model (GIM) previously presented by Le Caër *et al* [31]. We consider a local property such as the electric field gradient (EFG), which can be represented by a symmetric second-rank tensor $\mathcal{V}$. The components of $\mathcal{V}$ can be represented for our purposes by the trace $\mathrm{Tr}(\mathcal{V})$ and the five real quantities $T_i, i=1,\ldots,5$ directly deduced from the irreducible spherical tensor associated with $\mathcal{V}$ [36,66,67]. These are given by

$$T_\alpha = \sqrt{\tfrac{1}{3}}\mathrm{Tr}(\mathcal{V}) = \sqrt{\tfrac{1}{3}}(V_{xx}+V_{yy}+V_{zz}) \tag{A1a}$$

$$T_1 = \sqrt{\tfrac{2}{3}}[V_{zz} - \tfrac{1}{2}(V_{xx}+V_{yy})] \tag{A1b}$$

$$T_2 = \sqrt{\tfrac{1}{2}}(V_{xx}-V_{yy}) \tag{A1c}$$

$$T_3 = \sqrt{2}V_{yz} \tag{A1d}$$

$$T_4 = \sqrt{2}V_{xz} \tag{A1e}$$

$$T_5 = \sqrt{2}V_{xy}. \tag{A1f}$$

In equations (A1), we have not assumed that $\mathcal{V}$ is diagonal nor any special relationship in magnitudes between V_{xx}, V_{yy} and V_{zz}. For the case of an EFG, we can further restrict ourselves to a zero-trace tensor, so that $T_\alpha = 0$. It is then convenient to define the modulus S of the tensor $\mathcal{V}$ as

$$S^2 = \sum_{i,j=x,y,z} S_{i,j}^2 = \sum_{i=1}^{5} T_i^2. \tag{A2}$$

The Gaussian independent model is based on two necessary and sufficient hypotheses. The first is given by:

(H1) The solid under study is isotropic on average: that is the tensor $\mathcal{V}$ is statistically invariant under any orthogonal transformation [36, 68]

$$\mathcal{V} \rightarrow \mathcal{V}' = C^{\mathrm{T}}\mathcal{V}C \tag{A3}$$

where C is a general real orthogonal matrix.

We obtain certain conditions on the distribution over the quantities T_i by averaging the T_i over all possible orientations. These are given by

$$\begin{aligned} &\langle T_i \rangle = 0 \\ &\langle T_i T_j \rangle = 0, i \neq j \\ &\langle T_i^2 \rangle = \frac{1}{5}\langle S^2 \rangle = \sigma^2 \end{aligned} \tag{A4}$$

where S was the modulus of the tensor $\mathcal{V}$. In other words, the variance-covariance matrix Λ of the random variables T_i is given by

$$\Lambda = \tfrac{1}{5}\langle S^2 \rangle I_5 \tag{A5}$$

where I_5 is the unit matrix of order 5.

The second hypothesis is given by:

(H2) The distribution of the various elements V_{ij} is multivariate normal.

This means that the joint distribution $P(T_1, \ldots T_5)$ must be of product form for the different distributions of $T_i, i = 1, \ldots, 5$ taken individually in order to satisfy (H1) and (H2), these must be normal (Gaussian) distributions. Then the joint distribution $P(T_1, \ldots, T_5)$ must be of the form

$$P(T_1, \ldots, T_5) = \left(\frac{1}{2\pi\sigma^2}\right)^{5/2} \exp\left(-\frac{S^2}{2\sigma^2}\right) \tag{A6}$$

where σ is the standard deviation of the distribution for each of the T_i. The square modulus S^2 is given by the sum of the squares of five independent random variables

with zero mean and all with the same variance σ_S^2. This means that the distribution for S^2/σ^2 must be given by the chi-square distribution with five degrees of freedom, or

$$P_5(S) = \frac{1}{3}\sqrt{\frac{2}{\pi}}\frac{S^4}{\sigma^5}\exp\left(-\frac{S^2}{2\sigma^2}\right). \tag{A7}$$

This is the same as equation (4) for the distribution of Δ, $P(\Delta)$, as obtained from the Czjzek *et al* shell model. The numerical parameter expressing the width of the distribution σ introduced by Czjzek is seen to be given by

$$\sigma^2 = \tfrac{1}{5}\langle\Delta^2\rangle \tag{A8}$$

where σ given above is the standard deviation of the distribution of the factors T_i.

Le Caër *et al* [40] have also obtained the expression $P(q,\eta)$ given in equation (1). This model distribution is thus shown to have a much wider validity than the point charge simulations of Czjzek *et al* would at first indicate. Certain averages over $P(q,\eta)$ are useful in practical applications. The average over only the positive (negative) values of q of the marginal distribution $Q(q)$ gives

$$\langle q_\pm\rangle/\sigma_{q\pm} = \pm 3.067 \tag{A9a}$$

$$p_+ = p_- = 0.5 \tag{A9b}$$

where $p_\pm$ is the area under the positive (negative) part of $P(q,\eta)$. The average over the distribution of the modulus S gives

$$\langle S\rangle/\sigma_S = 3.094 \tag{A10}$$

where σ_S is the standard deviation of S. The averages over $R(\eta)$ give:

$$\langle\eta\rangle = 0.610 \tag{A11a}$$

$$\sigma_\eta = 0.243 \tag{A11b}$$

where σ_η is the standard deviation of η, and this value of $\langle\eta\rangle$ has been used in exploiting the experimental spectra.

The two hypotheses (H1) and (H2) do not depend upon the detailed mathematical form of the elements of the tensor $\mathcal{V}$ (which is here taken as the EFG tensor, but could also be the tensor of local strains; see [40]). We note that the EFG distributions simulated by Pustowka *et al* [69] for a random distribution of point defects on cubic and hexagonal lattices show a great similarity to the GIM distribution for a high concentration of defects (0.3 to 0.5). The same result was obtained analytically by Stockmann [70] for a cubic lattice. In this case, the lattice remains perfectly cubic with respect to orientational order. These results show that the observation of the GIM distribution does not allow us to conclude that the system studied is describable as a random packing of shells with no chemical order. An experimenter who knows nothing about the sample under study except that the distribution follows the GIM form cannot know if the sample is amorphous or crystalline. At most the conclusion that disorder is present in the sample is allowed.

References

[1] Shechtman D, Blech I, Gratias D and Cahn J W 1984 *Phys. Rev. Lett.* **53** 1951–3
[2] Sadoc A, Flank A M, Lagarde P, Sainfort P and Bellissent R 1986 *J. Physique* **47** 873–7
[3] Sadoc A 1986 *J. Physique Coll.* **47** C8 1003–8
[4] Sadoc A, Lagarde P and Sainfort P 1987 *Int. J. Mod. Phys.* B **1** 133–50
[5] Sadoc A, Flank A M and Lagarde P 1988 *Phil. Mag.* B **57** 399–410
[6] Warren W W Jr, Chen H S and Hauser J J 1985 *Phys. Rev.* B **32** 7614–6
[7] Warren W W Jr, Chen H S and Espinoza G P 1986 *Phys. Rev.* B **34** 4902–5
[8] Swartzendruber L J, Shechtman D, Bendersky L and Cahn JW 1985 *Phys. Rev.* B **32** 1383–5
[9] Eibschütz M, Chen H S and Hauser J J 1987 *Phys. Rev. Lett.* **56** 169–72
[10] Eibschütz M, Lines M E, Chen H S, Waszczak JV and Papaefthymion G 1987 *Phys. Rev. Lett.* **59** 2443–6
[11] Schurer P J, Koopmans B, van der Woude F and Bronsveld P 1986 *Solid State Commun.* **59** 619–3
[12] Wang K, Garoche P and Calvayrac 1988 *J. Physique Coll.* **49** C8 237–8
[13] Hauser J J, Chen H S and Waszczak 1986 *Phys. Rev.* B **33** 3577–80
[14] Bellissent R, Hippert F, Monod P and Vigneron P 1987 *Phys. Rev.* B **36** 5540–3
[15] Yamane H, Kimura K, Shibuya T and Takeuchi S 1987 *Mater. Sci. Forum* **22–24** 539–54
[16] Bancel J M and Heiney P A 1986 *Phys. Rev.* B **33** 7917–22
[17] Bendersky L 1985 *Phys. Rev. Lett.* **55** 1461–63
[18] Robinson K 1952 *Acta Crystallogr.* **5** 397–403
[19] Cooper M and Robinson K 1966 *Acta Crystallogr.* **20** 614–7
[20] McAlister A J, Bendersky L A, Schaefer R J and Biancaniello F S 1987 *Scripta Metall.* **21** 103–106
[21] Tibballs J E, Davis R L and Parker B A 1989 *J. Mater. Sci.* **24** 2177–82
[22] Nicol A D I 1953 *Acta Crystallogr.* **6** 285–93
[23] Robertson J L, Misenheimer M E, Moss S C and Bendersky L A 1986 *Acta Metall.* **34** 2177–89
[24] Tanaka M, Terauchi M, Suzuki S, Hiraga K and Hirabayashi M 1987 *Acta Crystallogr.* B **43** 494–501
[25] Chen H S, Koskenmaki D and Chen C H 1987 *Phys. Rev.* **35** 3715–21
[26] Janot Ch, Dubois J M and Pannetier J 1987 *Mater. Sci. Forum* **22-24** 329–44
[27] Kaufman M J and Melmed A J 1987 *Phil. Mag. Lett.* **56** 129–34
[28] Lasjaunias J C, Tholence J L, Berger C and Pavuna D 1987 *Solid State Commun.* **64** 425–9
[29] Hauser J J, Chen H S, Espinosa G P and Waszczak J V 1986 *Phys. Rev.* B **34** 4674–8
[30] Dunlap R A, O'Handley R C, McHenry M E and Chatterjee R 1988 *Phys. Rev.* B **37** 8484–7
[31] Le Caër G, Brand R A and Dubois J M 1987 *Phil. Mag. Lett.* **56** 143–51
[32] Stadnik ZM, Stroink G, Ma H and Williams G 1989 *Phys. Rev.* B **39** 9797–805
[33] Gupta A and Jayaraj ME 1989 *Phys. Rev.* **39** 8757–9
[34] Koopmans B, Schurer P J and van der Woude F 1987 *Phys. Rev.* B **35** 3005–8
[35] Xu R, Werkman R D, Vince I, Schurer P J and van der Woude F 1988 *Hyperfine Interact.* **45** 403–7
[36] Czjzek G, Fink J, Götz F, Schmidt H, Coey J M D, Rebouillat J-P and Liénard A 1981 *Phys. Rev.* **23** 2513–30
[37] Le Caër G, Brand R A and Dehghan 1984 *J. Physique Coll.* **46** C8 149–73
[38] Scholte P M L O, Tegze M and van der Woude F 1988 *Phys. Rev.* B **38** 12929–36
[39] Le Caër G, Brand R A and Dubois J M 1988 *Hyperfine Interact.* **42** 943–6
[40] Le Caër G, Dubois J M and Brand R A 1984 *Amorphous Metals and Nonequilibrium Processing—MRS Europe 1984* ed von Allmen (Paris: J. Physique) pp 249–54
[41] Zirnbauer M, Verbaarschot J and Weidemuller H A 1983 *Nucl. Phys.* A **411** 161–173
[42] Palmer R G and Pond C M 1979 *J. Phys. F: Met. Phys.* **9** 1451–1459
[43] Levi Yeyati A, Weissmann M and López García A 1988 *Phys. Rev.* **37** 10608–11
[44] Mackay AL 1981 *Sov. Phys. Crystallogr.* **26** 571–2 (*Kristallografiya* **26** 910–9)
[45] Mackay AL 1982 *Physica* A **114** 609–13
[46] Mackay AL 1986 *Comput. Math. Appl.* B **12** 21–37
[47] Brand R A, Le Caër G, Dubois J M, Hippert F, Sauer Ch and Pannetier J 1990 *J. Phys.: Condens. Matter* **2** 3855–66
[48] Dubois J M, Janot Ch and Pannetier J 1986 *Phys. Lett.* **115A** 177–181
[49] Janot Ch, Pannetier J, Dubois J M and Fruchart R 1986 *Phys. Lett.* **119A** 309–12

[50] Ruebenbauer K and Birchall T 1979 *Hyperfine Interact.* **7** 125–33
[51] Blaes N, Fisher H and Gonser U 1985 *Nucl. Instrum. Methods* B **9** 201–8
[52] Hesse J and Rübartsch 1974 *J. Phys. E: Sci. Instrum.* **7** 526–32
[53] Le Caër G, Dubois J M, Fisher H, Gonser U and Wagner H G 1984 *Nucl. Instrum. Methods* B **5** 25–33
[54] Brand R A 1987 *Nucl. Instrum. Methods* B **28** 398–416
[55] Brand R A and Le Caër G 1988 *Nucl. Instrum. Methods* B **34** 272–284
[56] Greneche J M and Varret F 1982 *J. Physique Lett.* **43** L233–37
[57] Falkenhagen G and Hofman W 1952 *Z. Metallkde.* **43** 69–81
[58] Nasu S, Gonser U, Shingu P H and Murakami Y 1974 *J. Phys. F: Met. Phys.* **4** L24–31
[59] Janot Ch, Pannetier J, Dubois J M, Houin J P and Weinland P 1988 *Phil. Mag.* B **58** 59–67
[60] Henley C 1986 *Phys. Rev.* B **34** 797–816
[61] Janot Ch, Dubois J M and Pannetier J 1987 *Physica* **146B-C** 351–72
[62] Dubois J M, Pannetier J and Janot Ch 1987 *Mater. Sci. Forum* **22–24** 311–28
[63] Janot Ch and Dubois J M 1988 *J. Phys. F: Met. Phys.* **18** 2303–43
[64] Janot Ch, de Boissieu M, Dubois J M and Pannetier J 1989 *J. Phys.: Condens. Matter* **1** 1029–48
[65] Janot Ch, Dubois J M, Pannetier J, de Boissieu M and Fuchart R 1988 *Quasicrystalline Materials* ed Ch Janot and J M Dubois (Singapore: World Scientific) pp 107–25
[66] Egami T and Strolovitz D 1982 *J. Phys. F: Met. Phys.* **12** 2141–63
[67] Jerphagnon J, Chemla D and Bonneville R 1978 *Adv. Phys.* **27** 609–51
[68] Metha MN 1967 *Random Matrices* (New York: Academic)
[69] Pustowka A J, Sawicka B D and Sawicki J A 1973 *Phys. Status Solidi* b **57** 783–91
[70] Stockmann HJ 1981 *J. Magn. Reson.* **44** 145–58